

Design and Implementation of PI and Droop Control for a Three-Phase System Using Simulink and Simscape

AUTHOR: RASHIDA OLOMOWEWE

CONTRIBUTOR: MORRIS TAMBAH NYANTEE

August 1, 2025

ADVISORS:

Prof. Serge Pierfederici

Prof. Milad Bahrami

Work conducted as a summer internship in LEMTA Lab

Contents

Abstract	3
1 Introduction	4
1.1 Objectives	4
2 System Modeling and Control Design	5
2.1 Derivation of System Equations	5
2.1.1 Transformation from abc Frame to $\alpha\beta$ Frame (Clarke Transformation) .	5
2.1.2 Transformation from $\alpha\beta$ Frame to dq Frame (park Transformation) . .	6
2.2 Control-Oriented Modeling	6
2.3 PI Inner Controller Design	7
2.3.1 Inner Voltage Controller	7
2.3.2 Inner Loop Current Controller	8
2.4 Three-Phase System Modeling	9
2.5 Droop Control Design	9
2.6 System Overview Design	11
3 Simulation Procedure	12
4 Result and Discussion	13
4.1 Simulation of three-phase System modeling setup	13
4.1.1 Observation	14
4.1.2 Theoretical Validation:	14
4.2 PI inner Controllers with Three-Phase System	14
4.2.1 Observation	15
4.3 PI Control with Droop and Three-Phase System	15
5 Conclusion	18
6 Future Works	19
A Appendix A: System Dynamics Function Block	20

Abstract

A control system for a three-phase power converter was developed and validated using MATLAB Simulink and Simscape. The objective was to design a robust voltage and current control strategy, simulate system dynamics, and implement performance enhancements through different control methods such as PI and droop control. The development process began with the derivation of the governing equations for the voltage of the capacitor (V_{cdq}), the current of the inductor (I_{dq}), and the verification was carried out using step inputs in a simplified system model

Following this, the inner-loop current and capacitor voltage control equations were derived and then linearized to enable the design of a proportional-integral (PI) controller. The controller was implemented based on the linearized model, with system parameters such as gain and time constants calculated accordingly. The inner control loops were first implemented and tested independently to verify their performance using step reference signals.

To extend the controller to a full three-phase implementation, the three-phase system was modeled in Simscape and the three-phase voltage and current signals (V_{abc} , I_{abc} , I_{Labc}) were transformed into the DQ reference frame using Clarke and Park transformations. This conversion enabled the application of the PI controller to regulate the three-phase system using steady-state DC-like signals. Following successful integration, a droop control mechanism was designed and implemented to enhance system stability. The combined PI and droop control schemes were tested under varying load conditions, demonstrating the effective regulation and dynamic performance of the three-phase system.

1 Introduction

As modern power systems integrate more renewable energy sources based on inverter technology, maintaining grid stability without synchronous generators has become a growing challenge. Grid-forming inverters (GFMI) are proposed as a solution, capable of regulating voltage and frequency independently. This project aims to design and simulate a GFMI with droop control and PI-based current regulation. The goal is to assess its ability to maintain stable operation and support grid dynamics under standalone conditions.

1.1 Objectives

- To design and implement the inner PI-based current controller in the dq -frame, and test its performance under step inputs and steady-state conditions.
- To model a three-phase inverter system with an LCL filter in MATLAB/Simulink and integrate it with the inner controller.
- To develop a droop-based outer control loop for generating voltage and frequency references.
- To validate that the generated V_{cdqref} aligns with the capacitor voltage V_{cdq} , confirming correct operation of the overall control strategy.

2 System Modeling and Control Design

2.1 Derivation of System Equations

To design effective control strategies for a three-phase transmission system, it is crucial to begin with a clear mathematical representation of its behavior. Starting from the physical structure, which includes line inductances, shunt capacitances, and load components, the differential equations that govern the voltages and currents of the system were derived in the time domain.

These equations are initially formulated in the natural abc (three-phase) frame. To simplify control and analysis, the system is then transformed into the synchronous dq reference frame using Clarke and Park transformations. This process converts sinusoidal signals into steady-state DC quantities, enabling the decoupled control of capacitor voltages and inductor currents. The following is a schematic of the physical system. Then follow the corresponding derivation of its state-space equations in the dq frame.

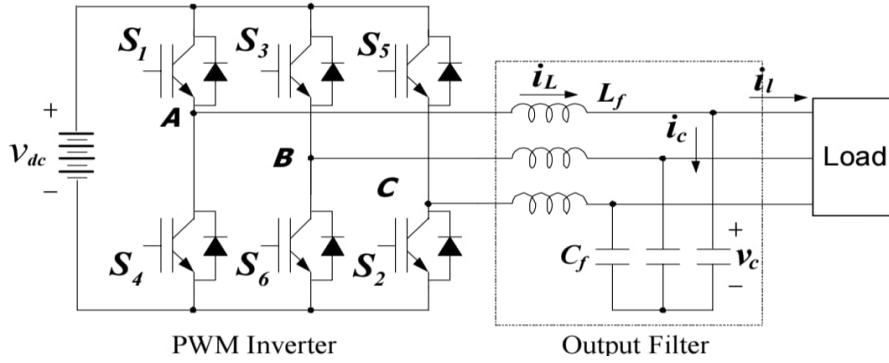


Figure 1: Three-phase inverter with an output LC filter. [2]

Figure 1 illustrates a standard three-phase voltage-source inverter equipped with an LC filter. The DC link is typically modeled as an ideal voltage source due to its relatively low impedance. The dynamic behavior of the LC filter can be described using Kirchhoff's laws as follows:

$$\frac{L di_{abc}}{dt} = V_{abc} - r i_{abc} - V_{c_{abc}} \quad (1)$$

$$\frac{C dV_{c_{abc}}}{dt} = i_{abc} - i_{L_{abc}} \quad (2)$$

Here, i_{abc} , V_{abc} , $V_{c_{abc}}$, and $i_{L_{abc}}$ represent the three-phase vectors of inductor current, line voltage, capacitor voltage, and load current, respectively.

2.1.1 Transformation from abc Frame to $\alpha\beta$ Frame (Clarke Transformation)

The transformation from the abc frame to the $\alpha\beta$ frame can be obtained by multiplying the quantity of abc by the Clark transformation matrix. In this report, it is denoted as the T_{32} matrix.

$$\begin{bmatrix} \alpha \\ \beta \end{bmatrix} = \frac{2}{3} \begin{bmatrix} 1 & -\frac{1}{2} & -\frac{1}{2} \\ 0 & \frac{\sqrt{3}}{2} & -\frac{\sqrt{3}}{2} \end{bmatrix} \begin{bmatrix} a \\ b \\ c \end{bmatrix}$$

$$T_{32} = \frac{2}{3} \begin{bmatrix} 1 & -\frac{1}{2} & -\frac{1}{2} \\ 0 & \frac{\sqrt{3}}{2} & -\frac{\sqrt{3}}{2} \end{bmatrix}$$

$$L \frac{d(T_{32}i_{abc})}{dt} = T_{32}\mathbf{V}_{abc} - rT_{32}\mathbf{i}_{abc} - T_{32}\mathbf{V}_{Cabc} \quad (3)$$

$$L \frac{d\mathbf{i}_{\alpha\beta}}{dt} = \mathbf{V}_{\alpha\beta} - r\mathbf{i}_{\alpha\beta} - \mathbf{V}_{C\alpha\beta} \quad (4)$$

2.1.2 Transformation from $\alpha\beta$ Frame to dq Frame (park Transformation)

The resulting equation in the $\alpha\beta$ frame can now be further transformed into the rotating reference frame dq , applying the Park transformation. The sinusoidal signals are converted into DC-like quantities under steady-state conditions. This greatly simplifies control design, particularly in vector control applications.

$$P(\theta) = \begin{bmatrix} \cos(\theta) & \sin(\theta) \\ -\sin(\theta) & \cos(\theta) \end{bmatrix} \quad (\text{Park Transformation})$$

$$L \frac{d(P(\theta)i_{\alpha\beta})}{dt} = P(\theta)\mathbf{V}_{\alpha\beta} - rP(\theta)\mathbf{i}_{\alpha\beta} - P(\theta)\mathbf{V}_{C\alpha\beta}$$

$$L \frac{d\mathbf{i}_{dq}}{dt} = \mathbf{V}_{dq} - r\mathbf{i}_{dq} - \mathbf{V}_{Cdq} + L\omega J\mathbf{i}_{dq} \quad (5)$$

where

$$J = \begin{bmatrix} 0 & 1 \\ -1 & 0 \end{bmatrix}$$

Applying the Clarke and Park transformations to the capacitor voltage equation (eq.2) in the abc frame yields the corresponding dq frame equation shown above. The additional term involving J accounts for the rotating reference frame.

$$C \frac{d\mathbf{V}_{Cdq}}{dt} = \mathbf{i}_{dq} - \mathbf{i}_{Ldq} + C\omega J\mathbf{V}_{Cdq} \quad (6)$$

2.2 Control-Oriented Modeling

In this GFMI Setup, there are two controllers setup:

- **Outer controller:** The outer control loop regulates the frequency and voltage magnitude based on active and reactive power output, respectively. This is derived from the power flow equations of a two-bus system, where active power primarily depends on the phase angle difference and reactive power depends on the voltage magnitude difference [1].

The controller uses droop equations to generate the reference frequency and voltage: the frequency reference is obtained by comparing the actual active power to a reference value, while the voltage reference is derived from the reactive power error through a PI controller. This outer loop allows the inverter to operate without communication, provides grid support, and ensures proper power sharing among parallel inverters.

- **Inner Controllers:** The inner control loop regulates the inverter terminal voltage by controlling the output current in the synchronous dq -frame. A current-mode control strategy is used, where the voltage reference from the outer loop is converted into current references through PI controllers. These are then compared with the measured currents, and the resulting errors are used to generate voltage control signals [1].

Feed-forward decoupling terms are applied to reduce the coupling between the d- and q-axes. The final control voltages are transformed into three-phase abc signals and sent to the inverter, enabling fast and stable current tracking.

2.3 PI Inner Controller Design

2.3.1 Inner Voltage Controller

To Obtain the Voltage controller Design the PI control derivative strategy was implemented:

$$\frac{CdV_{cdq}}{dt} = i_{dq} - iL_{dq} + CwJi_{dq} - \frac{V_{cdq}}{R_c} \quad (7)$$

Using Transforming to Linear:

$$i_{dq}^* = i_{dq} - ic_{dq} + CwJV_{cdq} \quad (8)$$

$$\frac{CdV_{cdq}}{dt} = i_{dq}^* - \frac{V_{cdq}}{R_c} \quad (9)$$

The plant transfer function can be obtained:

$$C(s)V_{cdq}(s) = I_{dq}(s) * -\frac{V_{cdq}}{R_c}(s) \quad (10)$$

$$\frac{I_{dq}(s)*}{V_{dq}(s)} = \frac{1}{\frac{1}{R_c} + C} \quad (11)$$

The Open Loop transfer function can be obtained: $C * T.F.$

$$\frac{kp * R_c}{\tau s} \quad (12)$$

The Closed-Loop Transfer Function Controller System:

$$\frac{1}{1 + \left(\frac{\tau s}{Kp * R_c} \right)} \quad (13)$$

Therefore:

$$kp = (X/R_c) \quad (14)$$

$$\tau s = R_c * C \quad (15)$$

Recalling Equation 8, plant equation can be represented as:

$$I_{dq} = I_{dq}^* + IL_{dq} - CwJV_{cdq} \quad (16)$$

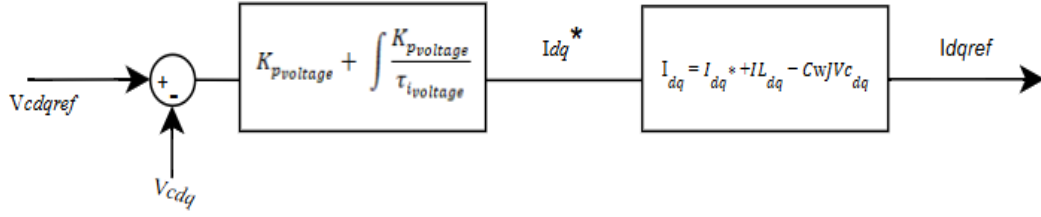


Figure 2: Voltage Controller

2.3.2 Inner Loop Current Controller

To Obtain the Current controller Design the PI control derivative strategy was implemented:

$$\frac{Ldi_{dq}}{dt} = V_{dq} - ri_{dq} - Vc_{dq} + LwJi_{dq} \quad (17)$$

Using Transforming to Linear:

$$V_{dq}^* = V_{dq} - Vc_{dq} + LwJi_{dq} \quad (18)$$

$$\frac{Ldi_{dq}}{dt} = V_{dq}^* - ri_{dq} \quad (19)$$

The plant transfer function can be obtained:

$$L(s)I_{dq}(s) = V_{dq}^*(s) - rI_{dq}(s) \quad (20)$$

$$\frac{I_{dq}(s)}{V_{dq}^*(s)} = \frac{\frac{1}{R}}{\tau s + 1} \quad (21)$$

The Open Loop transfer function can be obtained: C * T.F.

$$C = kp(1 + \frac{1}{\tau s}) \quad (22)$$

The open Loop Transfer Function

$$kp * (\frac{\frac{1}{R}}{\tau s}) \quad (23)$$

The Closed-Loop Transfer Function Controller System:

$$kp * (\frac{1}{\frac{\tau s * R}{kp} + 1}) \quad (24)$$

Therefore:

$$kp = (XR) \quad (25)$$

$$\tau s = \frac{L}{R} \quad (26)$$

Recalling Equation 18, plant equation can be represented as:

$$V_{dq} = V_{dq}^* + V_{cdq} - L\omega J i_{dq} \quad (27)$$

plant equation can be represented as:

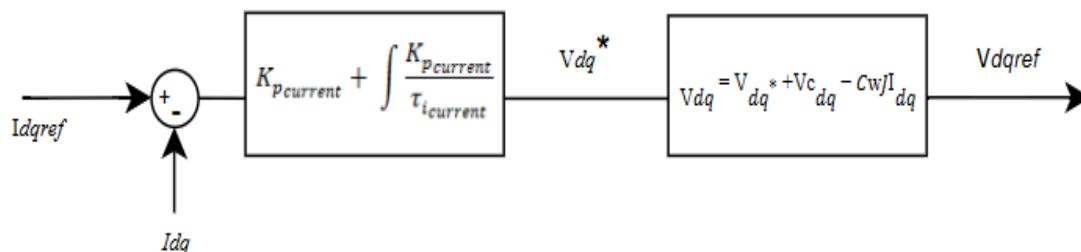


Figure 3: Current Controller

2.4 Three-Phase System Modeling

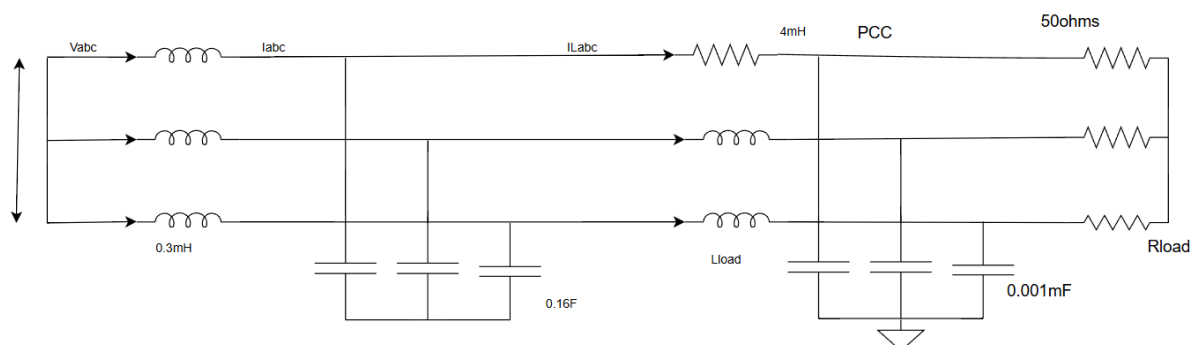


Figure 4: Schematic of the three-phase inverter system used in the simulation

The figure shows the three-phase inverter system used in this study. The inverter is connected to the load through an LCL filter, which consists of a $0.3mH$ inverter-side inductor, a $0.16mF$ grid-side Capacitor. An additional $4mH$ inductor is used to model the transmission path, and the load is represented by a resistive branch of 50Ω per phase with a small grounding capacitor of $0.001mF$. The system is modeled to observe voltage and current behavior at the Point of Common Coupling (PCC).

2.5 Droop Control Design

In this setup, the droop control functions as the outer controller. Active and reactive power of the inverter can be obtained using the voltage across the capacitor V_{cdq} as well as the Load Current IL_{dq} as seen in the equation below.

$$P_m = \frac{3}{2} * (V_{cd} IL_d + V_{cq} IL_q) \quad (28)$$

$$Q_m = \frac{3}{2} * (V_{c_q} I_{L_d} - V_{c_d} I_{L_q}) \quad (29)$$

The filtered Active and Reactive Power using low-pass filters is fed to the input of the droop control that is;

$$P_{filtered} = \frac{w_c}{w_c s + 1} * P_m \quad (30)$$

$$Q_{filtered} = \frac{w_c}{w_c s + 1} * Q_m \quad (31)$$

where:

- w_c : cut-off frequency

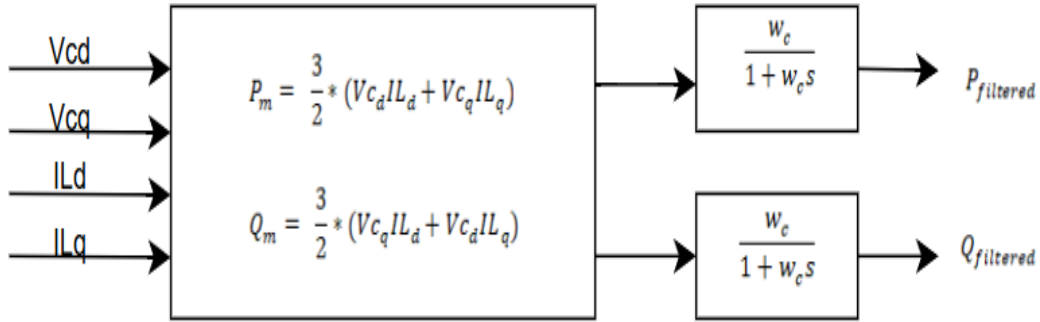


Figure 5: Output active and reactive power of the inverter.

For this set-up a frequency droop control was utilized. The control schemes are as seen below:

$$w_{droop} = w_{rated} - \frac{\Delta w}{P_{nominal}} * (P_{filtered} - P_{nominal}) \quad (32)$$

$$V_{droop} = v_{rated} - \frac{\Delta v}{Q_{nominal}} * (Q_{filtered} - Q_{nominal}) \quad (33)$$

The droop outputs w_{droop} and v_{droop} are filtered using a first-order filter. To obtain the inputs to the Inner controllers as well as the three phase system, inputs such as Θ as well as V_{cdq} are required. To obtain this:

$$\Theta = \int w_{droop} \quad (34)$$

$$V_{cdq} = v_{droop} * \sqrt{3} \quad (35)$$

Therefore, this parameters serve as variable to the system utilized for the control of the three phase system.

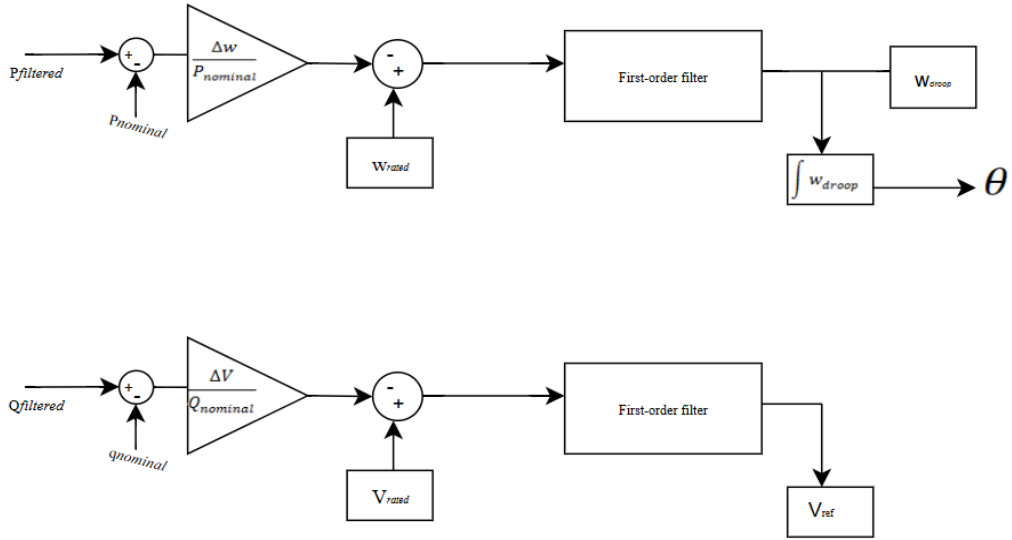


Figure 6: Outer control loop of the frequency-droop control scheme.

2.6 System Overview Design

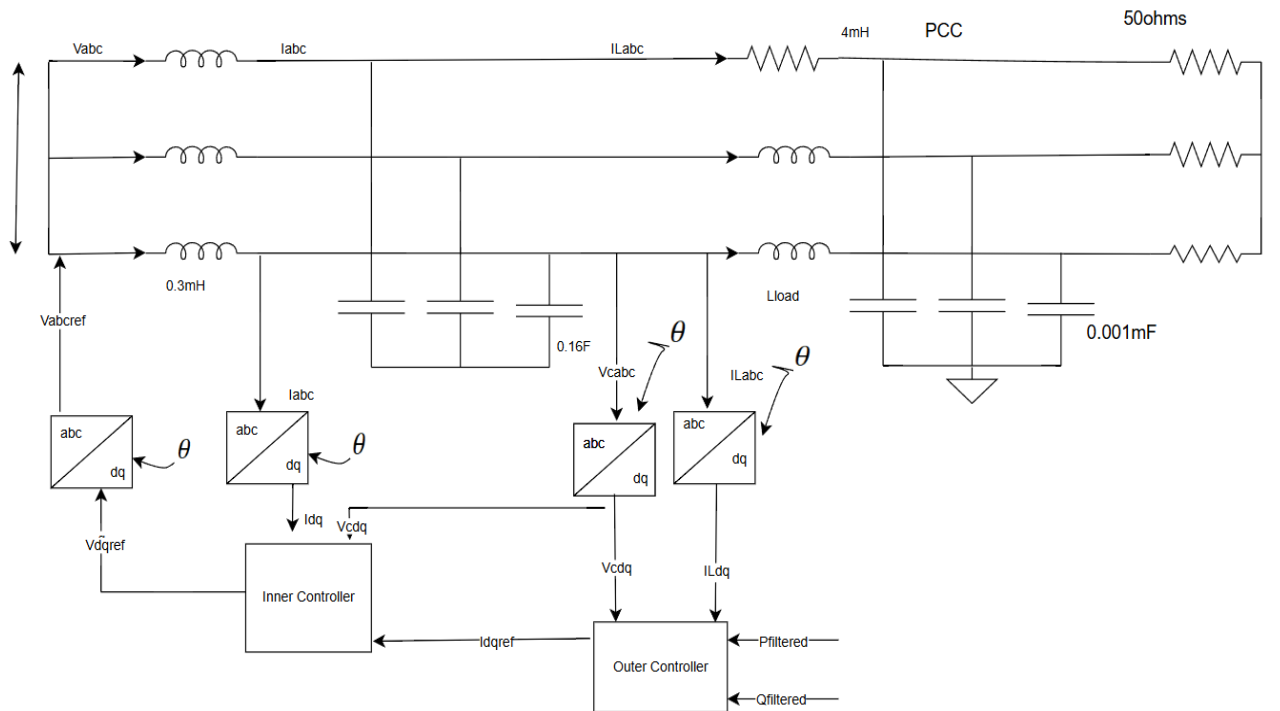


Figure 7: Whole System Model

3 Simulation Procedure

The simulation of the grid-forming inverter system was implemented in MATLAB/Simulink. The overall control architecture includes an outer droop controller and an inner current-mode PI controller operating in the synchronous dq -frame. The simulation procedure follows the steps below:

1. **System setup:** A three-phase inverter is connected to the grid through an LCL filter and resistive load. The system is modeled in the synchronous reference frame using *simscape*.
2. **Power calculation:** The inverter output active power P and reactive power Q are calculated using the inverter-side capacitor voltages V_{cdq} and inductor currents I_{ldq} in the dq -frame.
3. **Droop control:** The measured power values are used in droop equations to compute the frequency deviation and voltage magnitude deviation. The frequency reference is integrated to obtain the phase angle θ , which defines the rotational transformation.
4. **Voltage reference generation:** The droop-generated voltage magnitude V_{ref} is scaled by $\sqrt{3}$ to obtain the direct and quadrature voltage references V_{cdref} and V_{cqref} , which are used as inputs to the voltage controller.
5. **Outer voltage PI control:** The voltage references are compared with the measured capacitor voltages V_{cd} and V_{cq} , and the errors are processed through PI controllers to generate current references i_{dref} and i_{qref} .
6. **Inner current PI control:** The current references are compared with the actual inverter currents i_d and i_q , and the errors are passed through PI controllers to generate the control voltages v_{dref} and v_{qref} .
7. **Decoupling and transformation:** Feed-forward decoupling terms are added to reduce coupling between the d- and q-axes. The resulting voltages are then transformed from the dq -frame to the three-phase abc -frame using the calculated phase angle θ .
8. **Voltage application:** The three-phase voltages v_{abc} are applied to the inverter terminals, completing the closed-loop control process.

4 Result and Discussion

This section presents the simulation results of the grid-forming inverter system under three stages of development. First, the initial three-phase system is modeled and validated using steady-state dq-frame equations. Next, the performance of the inner PI-based voltage controller is evaluated using a step response. Finally, the complete system is tested with the outer droop controller to confirm proper voltage reference generation and tracking. The results validate both the control structure and the theoretical model.

4.1 Simulation of three-phase System modeling setup

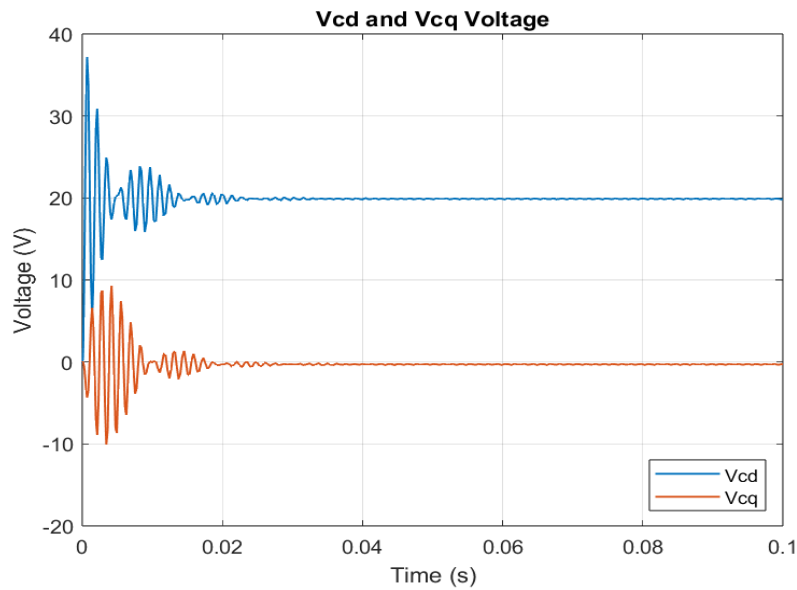


Figure 8: Simulated output of capacitor voltages V_{cdq} in the dq frame.

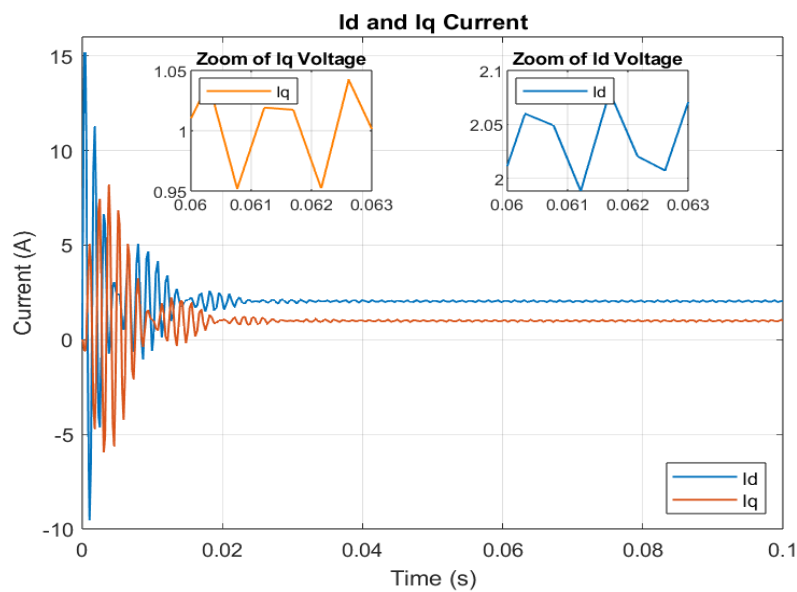


Figure 9: Simulated inductor currents in the I_{dq} frame.

4.1.1 Observation

- From Fig. 8, the voltage V_{cdq} remains constant and close to the reference 20 V and 0 V, validating that the capacitor voltage loop is well-regulated in the dq-frame.
- In Fig. 9, both I_{dq} reach steady-state values, confirming the correctness of the dq-frame current dynamics.

Minor ripples observed are due to system dynamics and switching behavior but remain within acceptable bounds.

4.1.2 Theoretical Validation:

The simulated values of $i_d = 2$ A, $i_q = 1$ A, and $V_{cd} = 20$ V were used to theoretically verify the dq-frame voltage equation. Using the expression at steady state:

$$V_d = Ri_d - \omega Li_q + V_{cd}$$

and the parameters $R = 0.1 \Omega$, $L = 300 \mu\text{H}$, and $\omega = 314.16$ rad/s, we obtain:

$$V_d = 0.1 \times 2 - 314.16 \times 0.0003 \times 1 + 20 = 0.2 - 0.09425 + 20 = 20.10575 \text{ V}$$

This result is in close agreement with the simulation input of $V_d = 20$ V, thereby validating the mathematical model of the system.

4.2 PI inner Controllers with Three-Phase System

A step reference was applied to the input of the inner d-axis voltage controller to assess its tracking performance. The reference V_{cdref} changed from 50 V at $t = 0$ s to 110 V at $t = 3$ s, while V_{cqref} was kept at 0 V. The resulting capacitor voltages V_{cd} and V_{cq} were used to evaluate the controller's ability to track setpoints and maintain axis decoupling.

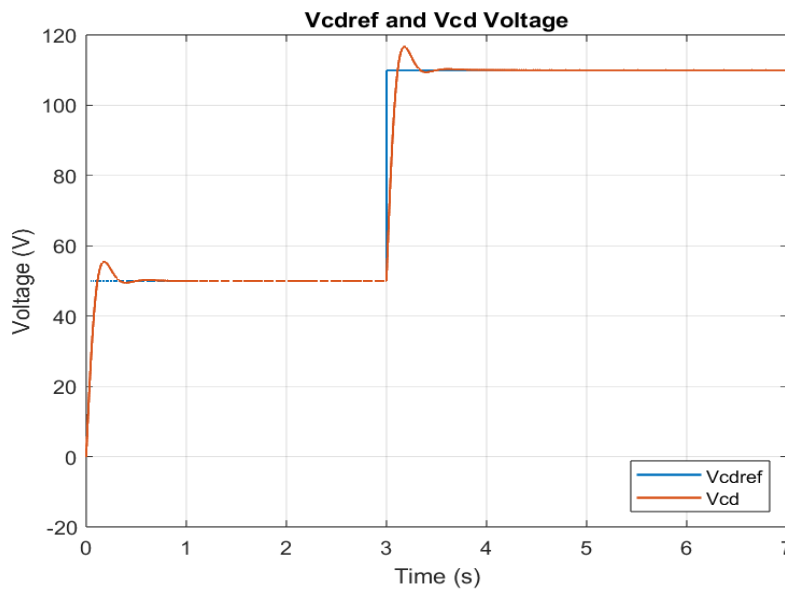


Figure 10: Comparison of the q-axis capacitor voltage V_{cd} and its reference V_{cdref} at the input of the inner voltage controller

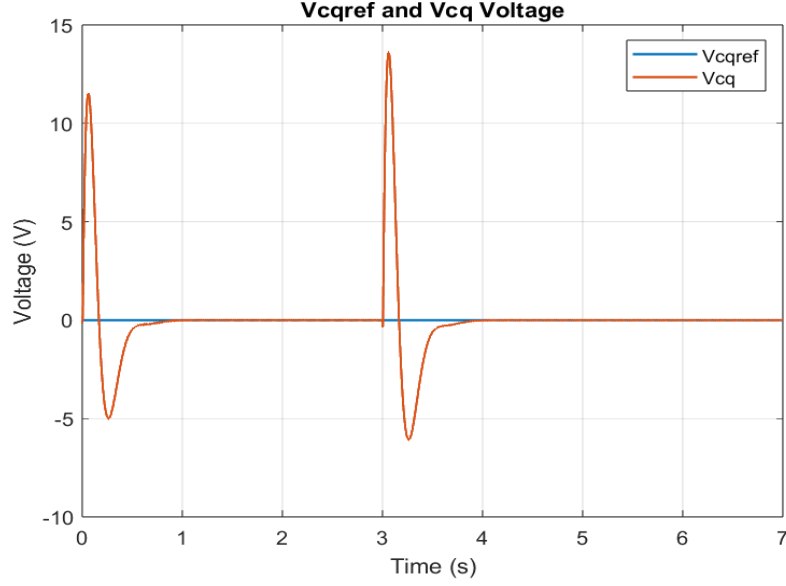


Figure 11: Comparison of the q-axis capacitor voltage V_{cq} and its reference V_{cqref} at the input of the inner voltage controller

4.2.1 Observation

The results demonstrate that the capacitor voltages V_{cd} and V_{cq} accurately track their respective reference values V_{cdref} and V_{cqref} . At $t = 0$ s, V_{cd} quickly settles around 50 V, and at $t = 3$ s, it successfully follows the step increase to 110 V. The V_{cq} voltage remains near zero throughout the simulation, confirming effective axis decoupling and proper performance of the dq-frame voltage controller.

4.3 PI Control with Droop and Three-Phase System

The reference voltage V_{cdref} was generated using the droop control equation based on system loading. With $P_{nominal} = 3000$ W and a frequency deviation $\Delta\omega = 0.05 \times 2\pi \times 60 = 18.85$ rad/s, the active power droop coefficient was set to $m = 6.28 \times 10^{-3}$ rad/sW.

For reactive power sharing, $Q_{nominal} = 500$ VAR and $\Delta V = 0.05 \times 110 = 5.5$ V yielded a reactive power droop coefficient of $n = 0.011$ V/VAR. These values determined the reference voltages V_{cdref} and V_{cqref} , which were tracked by the inner PI-controlled voltage loops.

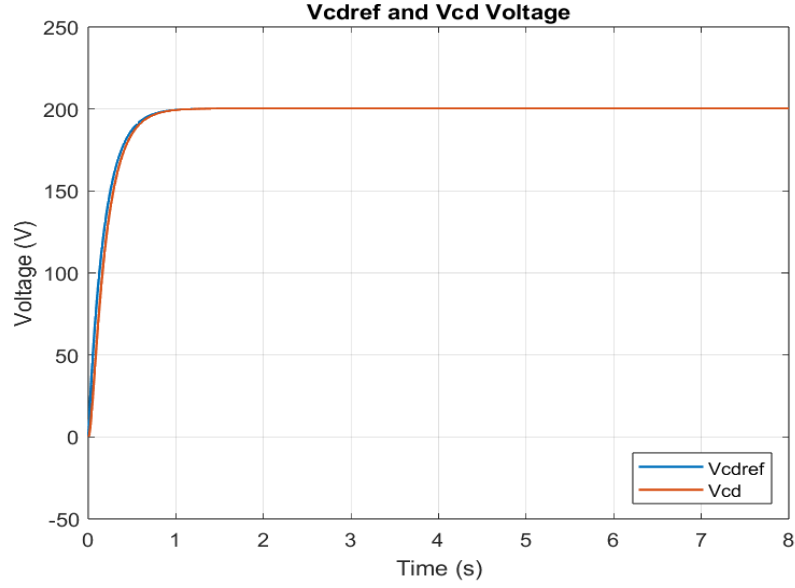


Figure 12: Tracking performance of V_{cd} with respect to the reference V_{cdref} under the enhanced droop control scheme

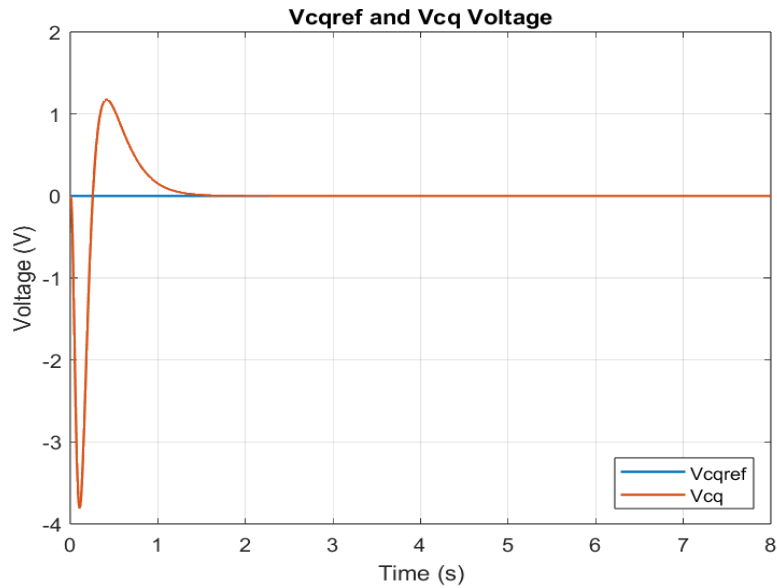


Figure 13: Tracking performance of V_{cq} with respect to the reference V_{cqref} under the enhanced droop control scheme

Observation

- The results demonstrate that the capacitor voltages V_{cd} and V_{cq} accurately follow their respective reference values V_{cdref} and V_{cqref} , validating the performance of the enhanced droop control strategy.
- As shown in Fig. 12, at $t = 0$ s, V_{cd} rapidly rises and settles around 200 V, closely matching the reference with minimal overshoot and fast settling time. This indicates that the voltage control loop responds effectively to changes in the droop-generated reference.

- Meanwhile, the V_{cq} voltage remains tightly regulated around 0 V throughout the simulation, as illustrated in Fig. 13. This behavior highlights strong axis decoupling and accurate control of the quadrature-axis voltage component.
- These results confirm that the cascaded PI voltage and current controllers, in conjunction with droop control, provide stable and precise voltage regulation in the synchronous dq -frame.

5 Conclusion

This work successfully designed and implemented PI and droop control strategies for a three-phase grid-forming inverter, demonstrated using Simulink and Simscape. The control strategy effectively enabled decoupled regulation of voltage and current in the synchronous dq frame. Simulation results confirm accurate voltage regulation, effective axis decoupling, and stable power-sharing performance, validating the robustness of the proposed control architecture under dynamic conditions.

The incorporation of the droop controller further enhanced system performance by enabling effective control, improving utilization, and reducing harmonic distortion. Theoretical considerations, including the analogy with conventional synchronous generator behavior, provided a solid foundation for modeling and implementation.

6 Future Works

This study focused on the implementation and validation of a grid-forming inverter (GFMI) under single-inverter operation and ideal load conditions. The performance of the controller was evaluated based on voltage tracking and power-sharing characteristics.

For future work, the system can be extended to include multiple grid-forming inverters operating in parallel. This would allow the evaluation of power-sharing accuracy, stability under grid disturbances, and robustness of the control strategy in multi-inverter configurations. Additionally, testing the controller performance under varying and nonlinear load conditions would provide further insights into the controller's adaptability and dynamic response.

A Appendix A: System Dynamics Function Block

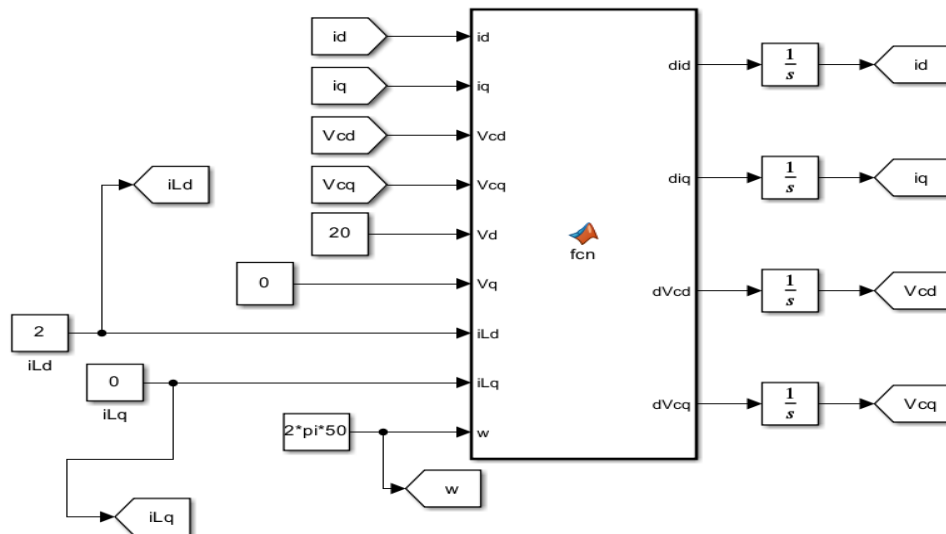


Figure 14: System modeling of the three-phase inverter setup, illustrating component interconnections and signal flow in the control architecture.

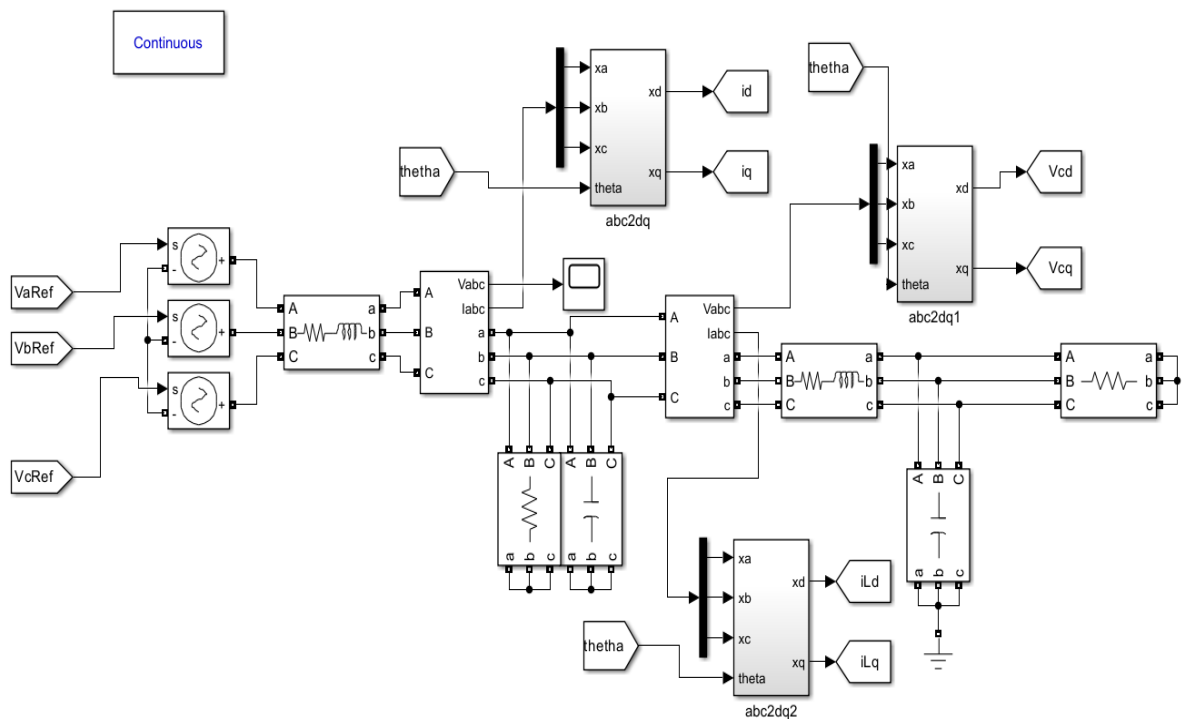


Figure 15: Simulink model of the complete three-phase inverter system with LCL filter.

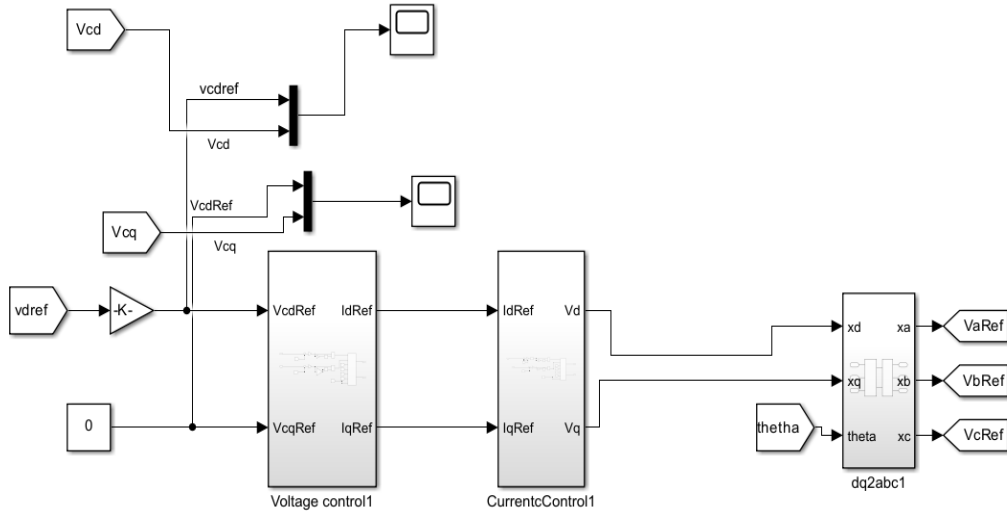


Figure 16: Simulink implementation of the inner and outer control loops, including PI controllers for voltage and current regulation within the dq frame.

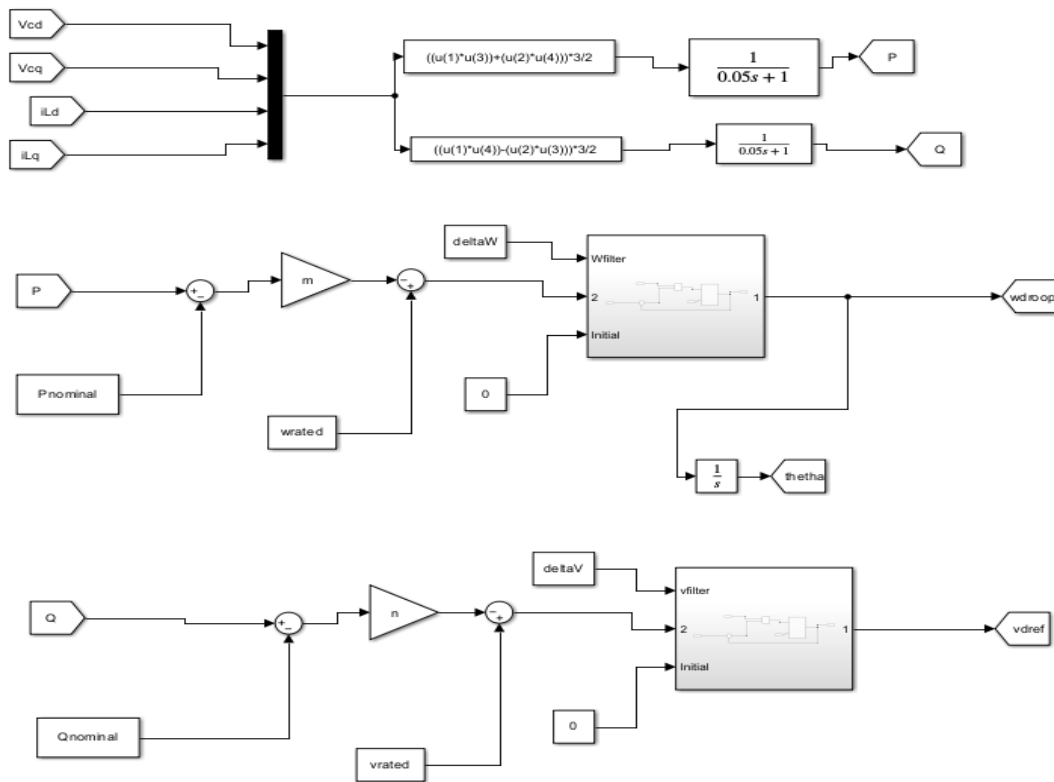


Figure 17: Simulink model of the droop controller used for generating dynamic voltage and frequency references based on power measurements.

References

- [1] M. Mirmohammad and S. P. Azad, “Control and stability of grid-forming inverters: A comprehensive review,” *Energies*, vol. 17, Art. no. 3186, Jun. 2024, doi: 10.3390/en17133186. :contentReference[oaicite:2]index=2
- [2] J. S. Lim, C. Park, J. Han, and Y. I. Lee, “Robust tracking control of a three-phase DC–AC inverter for UPS applications,” *IEEE Transactions on Industrial Electronics*, vol. 61, no. 8, pp. 4142–4151, Aug. 2014, doi: 10.1109/TIE.2013.2284155. :contentReference[oaicite:3]index=3